Journal of Ship Production and Design, Vol. 31, No. 2, May 2015, pp. 88-99(12)
https://doi.org/10.5957/JSPD.31.2.130046

A Method for Propeller Blade Optimization and Cavitation Inception Mitigation

Brenden Epps[†](✉), Oscar Víquez[‡], and Chryssostomos Chryssostomidis[‡]

[†]Fluid Energy Laboratory, Thayer School of Engineering, Dartmouth College, Hanover, NH, USA
[‡]Sea Grant Design Laboratory, MIT, Cambridge, MA, USA

Propeller blade design for fast ships is often driven by cavitation constraints. A tradeoff exists, where larger chord lengths and section thicknesses typically improve cavitation performance but result in lower efficiency. Typically, chord lengths are optimized for the design condition (ship endurance speed), with some specified margin to prevent cavitation off-design (at maximum ship speed). Cavitation performance at the maximum speed is considered post-facto, and blade shape often needs to be modified for cavitation considerations in high-speed operation.

This paper presents an improved method for blade shape optimization. The present method simultaneously considers the cavitation performance at the endurance speed design point and a maximum speed off-design point, and blade chord lengths and thicknesses are set to prevent cavitation at both operational conditions. During the present design optimization routine, the on-design load distribution is optimized, and the off-design performance is determined, such that the chord lengths can be set to a minimum that still prevents cavitation at both the on- and off-design conditions.

A case study is presented, considering the notional design of a propeller for the U.S. Navy DDG51 destroyer-class ship. Propellers designed using standard chord/thickness optimization procedures are compared to those designed using the present procedures. Cavitation performance is compared for the two design methods.

Keywords: propeller design, cavitation, blade optimization, chord length optimization, analytic bucket diagram

1.0 INTRODUCTION

We seek a deterministic approach for optimizing propeller blade chord and thickness in such a way as to maximize efficiency, provide requisite blade strength, and mitigate cavitation. For maximum efficiency, one desires zero chord lengths, since viscous losses scale with chord. However, structural considerations require finite chord and thickness, and increasing chord typically improves cavitation performance as well. So it is apparent that one can not arbitrarily choose the chord and thickness distributions but rather needs a deterministic optimization approach.

A number of design procedures exist to choose the chord and thickness distributions to prevent cavitation at a single design point, which either involve design tables (e.g. Brockett (1966)) or curve fits to these tables (e.g. Coney (1989)). However, these methods fail when multiple design points are considered. Herein, we consider the problem of optimizing loading for maximum efficiency at a ship's 20 knot *endurance speed* while optimizing the chord and thickness distributions to prevent cavitation at both the endurance speed and a 30 knot *maximum speed*. Since we aim to optimize the design at an off-design condition, the methods of Brockett (1966) and Coney (1989) do not apply, and we need a new method to optimize the blade shape to prevent cavitation.

This manuscript presents an improved design method that can be used to determine preliminary chord and thickness distributions for propeller blade design. The method employs propeller lifting line theory for the design optimization and analysis (Kerwin and Hadler, 2010), which is commonly used in the preliminary design phase. It is expected that the designer would then perform more advanced analyses using a panel method or CFD code (Kinnas et al, 2002; Brizzolara et al, 2010, e.g.). The aim of this work is to present a rapid, automated algorithm that will determine a preliminary design that closely matches the final output of these more sophisticated, time-consuming, manual analyses.

This article does not consider the case of a propeller operating in a non-uniform inflow. A non-uniform axial inflow presents a spatially-varying angle of attack between a propeller blade section and its free-stream inflow (axial inflow plus apparent rotational inflow). In this study, we do not consider variations in angle of attack due to spatially-varying axial inflow. Rather, we consider the case of angle of attack variation due to the propeller operating at two different advance coefficients (representing the endurance speed and maximum speed).

This paper is organized as follows: In §2.0, we review the theoretical foundation of the method. In §2.3, we develop an analytic equation to predict the cavitation performance of each 2D blade section. In §3.0, we develop a design procedure to optimize blade loading for maximum efficiency at an endurance speed while mitigating cavitation at a maximum speed. This procedure is illustrated in §4.0 in application the DDG51 destroyer-class vessel.

2.0 THEORY

2.1 Propeller lifting-line formulation

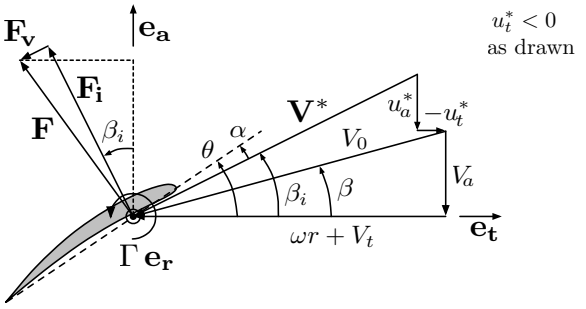

Figure 1: Propeller velocity diagram at radius r.

In *moderately-loaded* propeller lifting line theory (Lerbs, 1952; Epps and Kimball, 2013b), a propeller blade is represented by a vortex line, with trailing vorticity aligned to the local flow velocity (free-stream plus induced velocity). The induced velocities are computed using a vortex lattice, with helical trailing vortex filaments shed at discrete stations along the blade. The blade is also modeled as discrete vortex panels, having 2D section properties at each radius. Loads are computed by integrating the 2D section loads over the span.

Figure 1 illustrates the velocities and forces (per unit radius) on a 2D blade section: axial and tangential inflow velocities, V_a and V_t; axial and tangential induced velocities, u_a^* and u_t^*; and angular velocity ω. The total resultant inflow velocity has magnitude $V^* = \sqrt{(V_a+u_a^*)^2+(\omega r+V_t+u_t^*)^2}$ and is oriented at pitch angle β_i to the $\mathbf{e_t}$ axis. Also shown on Figure 1 are the angle of attack, α; blade pitch angle $\theta = \alpha+\beta_i$; circulation, Γ; inviscid Kutta-Joukowski lift force, $F_i = \rho V^*\Gamma$; and viscous drag force, $F_v = \frac{1}{2}\rho(V^*)^2 C_D c$, where ρ is the fluid density, C_D is the section drag coefficient, and c is the chord.

The 3D propeller geometry is built from given 2D section profiles that are scaled and rotated according to the chord length and the design point lift coefficient and inflow angle $\{c, C_{L_e}, \beta_{i_e}\}$ such that $C_L = C_{L_I} = C_{L_e}$ and $\alpha = \alpha_I$ at the (endurance speed) design point:

$$\left\{C_L, \alpha_I, \frac{f_0}{c}\right\} = \frac{C_{L_e}}{\widetilde{C}_{L_I}} \cdot \left\{\widetilde{C}_{L_I}, \widetilde{\alpha}_I, \frac{\widetilde{f}_0}{c}\right\} \tag{2.1}$$

$$\theta = \alpha_I + \beta_{i_e} \tag{2.2}$$

where C_{L_I} and α_I are the ideal lift coefficient and angle of attack, and the tilde values are the given profile (Abbott and Doenhoff, 1959).

The off-design performance of a propeller is computed using the method of (Epps, 2010). Each operating state is defined by the ship speed, V_s, rotation rate, ω, and unknown parameters $\{V^*, \alpha, C_L, \Gamma, u_a^*, u_t^*, \beta_i, \bar{u}_a^*, \bar{u}_t^*\}$. Since there are M vortex panels, there are $7M+2M^2$ unknowns and a system of as many non-linear equations. This system is solved using a Newton solver, which drives the following residual vector to zero (for each blade section).

$$\mathbf{R} = \begin{bmatrix} V^* & - & \sqrt{(V_a+u_a^*)^2+(\omega_m r_c+V_t+u_t^*)^2} \\ \alpha & - & (\alpha_I+\beta_{i_e}-\beta_i) \\ C_L & - & C_L(\alpha) \\ \Gamma & - & \left(\frac{1}{2}C_L V^* c\right) \\ u_a^* & - & \left([\bar{u}_a^*]\cdot[\Gamma]\right) \\ u_t^* & - & \left([\bar{u}_t^*]\cdot[\Gamma]\right) \end{bmatrix} \tag{2.3}$$

where $C_L(\alpha) \approx C_{L_e} + 2\pi(\alpha-\alpha_I)$ before stall and approximately constant post stall. Between solver iterations, $\{\beta_i, \bar{u}_a^*, \text{and } \bar{u}_t^*\}$ are updated. For each operating state, thrust, torque, and efficiency are easily calculated.

2.2 Cavitation

The *local cavitation number* is defined as

$$\sigma(r) \equiv \frac{p_{\text{atm}} + \rho g H - p_v}{\frac{1}{2}\rho(V^*(r))^2} \tag{2.4}$$

with atmospheric pressure $p_{\text{atm}} = 101$ kPa, seawater density $\rho = 1025$ kg/m^3, gravity $g = 9.81$ m/s^2, shaft centerline depth H, and vapor pressure $p_v = 2500$ Pa. The pressure coefficient (at radius r and chordwise location x) is

$$C_p(r,x) \equiv \frac{p(r,x) - (p_{\text{atm}} + \rho g H)}{\frac{1}{2}\rho(V^*(r))^2} \tag{2.5}$$

Since cavitation may occur when the pressure falls below the vapor pressure, chord must be made large enough such that the minimum pressure coefficient (i.e. maximum $-C_p$) satisfies

$$[-C_p]_{\max} \le \sigma \tag{2.6}$$

(Kerwin and Hadler, 2010).

Note that (2.4) represents the circumferential-average cavitation number for a particular radius, since the depth is taken as the shaft centerline depth, H. For a more conservative design requirement (2.6), one could compute the

cavitation number using the minimum depth seen by the blade section, $H-r$.

The minimum blade pressure, $[-C_p]_{\max}$, is a function of the blade loading $\{\Gamma, V^*, \alpha\}$ as well as the geometry $\{\theta, f_0, t_0, c\}$. Since the pitch and camber must be set to provide the required thrust loading at the endurance speed, the only tunable parameters (to prevent cavitation at the maximum speed) are the thickness and chord. In the following section, an analytic estimate of $[-C_p]_{\max}$ is derived, which can be used in conjunction with design constraint (2.6) to optimize thickness and chord.

2.3 An analytic estimate of $[-C_p]_{\max}$

In order to develop a deterministic design method that satisfies (2.6), we now formulate an analytic estimate of $[-C_p]_{\max}$. Employing Bernoulli's equation, (2.5) can be written as

$$-C_p(x) = \left\{ \frac{q(x)}{V^*} \right\}^2 - 1 \tag{2.7}$$

where $q(x)$ is the the total fluid velocity. For a 2D hydrofoil spanning $0 \le x \le c$, linear theory (with the Lighthill leading-edge correction) gives

$$\frac{q(x)}{V^*} = \left(1 + \frac{u_t(x)}{V^*} \pm \frac{u_c(x)}{V^*} \right) \sqrt{\frac{x}{x+\frac{1}{2}r_\ell}} \pm (\alpha - \alpha_I) \sqrt{\frac{c-x}{x+\frac{1}{2}r_\ell}} \tag{2.8}$$

where u_t and u_c are the perturbation velocities due to thickness and camber effects, respectively, and r_ℓ is the leading-edge radius.

A typical propeller blade section may be generated by superposition of a meanline form and thickness form for a given camber ratio f_0/c and thickness ratio

$$\tau \equiv \frac{t_0}{c}$$

For thin hydrofoils, the thickness perturbation velocity is proportional to the thickness ratio,

$$\frac{u_t(x)}{V^*} \approx a_1 \tau$$

Typical values of the constant a_1 are given in Table 1.

Table 1: Typical values of the constant a_1.

a_1	Thickness Form
$4/\pi \approx 1.27$	parabolic
1.20	NACA 65A
1.18	NACA 66

Similarly, the camber perturbation velocity can be assumed to be linearly proportional to the camber ratio,

$$\frac{u_c(x)}{V^*} \sim \frac{f_0}{c}$$

with the constant of proportionality depending on the meanline form. In lieu of determining these constants of proportionality, we note that the camber ratio is linearly proportional to the ideal lift coefficient for the section. For example, a NACA 'a'-series camber line scaled for ideal lift coefficient C_{L_I} has a camber perturbation velocity of

$$\frac{u_c(x)}{V^*} \approx \frac{1}{2} \frac{C_{L_I}}{(1+a)}$$

The leading edge radius is proportional to the square of the thickness ratio,

$$\frac{r_\ell}{c} = \rho_\ell \tau^2$$

where ρ_ℓ is the leading edge radius ratio for unit τ.

Combining these approximations for u_t and u_c, we can develop an analytic approximation for $-C_p(x)$. For the *upper* surface (suction side)

$$-C_p(x) \approx \left\{ A_1 \sqrt{\frac{x}{x+\frac{1}{2}r_\ell}} + A_2 \sqrt{\frac{c-x}{x+\frac{1}{2}r_\ell}} \right\}^2 - 1 \tag{2.9}$$

$$A_1 \equiv 1 + a_1\tau + \frac{1}{2}\frac{C_{L_I}}{(1+a)} \tag{2.10}$$

$$A_2 \equiv \alpha - \alpha_I \tag{2.11}$$

and for the *lower* surface (pressure side)

$$-C_p(x) \approx \left\{ A_3 \sqrt{\frac{x}{x+\frac{1}{2}r_\ell}} + A_4 \sqrt{\frac{c-x}{x+\frac{1}{2}r_\ell}} \right\}^2 - 1 \tag{2.12}$$

$$A_3 \equiv 1 + a_1\tau - \frac{1}{2}\frac{C_{L_I}}{(1+a)} \tag{2.13}$$

$$A_4 \equiv -(\alpha - \alpha_I) \tag{2.14}$$

Brockett (1966) created the cavitation bucket diagram (Figure 2), which plots $(\alpha - \alpha_I)$ versus $[-C_p]_{\max}$ for a particular camber ratio (i.e. fixed C_{L_I}) and thickness ratio ($\tau \equiv t_0/c$). These curves display three distinct regions:

Case 1: small net angle of attack (linear region). $[-C_p]_{\max}$ is located at $x/c \approx 1/2$ on the upper surface. Since $r_\ell/c \ll 1$, equation (2.9) reduces to

$$[-C_p]_{\max} \approx A_1^2 + 2A_1A_2 - 1 \tag{2.15}$$

which is indeed linearly-proportional to $(\alpha - \alpha_I)$.

Case 2: large positive net angle of attack (non-linear region). Setting, $\frac{d}{dx}([-C_p]_{\max}) = 0$ in (2.9) gives the location of $[-C_p]_{\max}$ on the upper surface

$$x/c = \frac{A_1^2}{A_1^2 + A_2^2(1 + 2c/r_\ell)^2} \tag{2.16}$$

Inserting (2.16) into (2.9) yields

$$[-C_p]_{\max} \approx A_1^2 + A_2^2(2c/r_\ell) - 1 \tag{2.17}$$

Comparing (2.15) and (2.17), case 2 is when $A_2 > A_1\, r_\ell/c$.

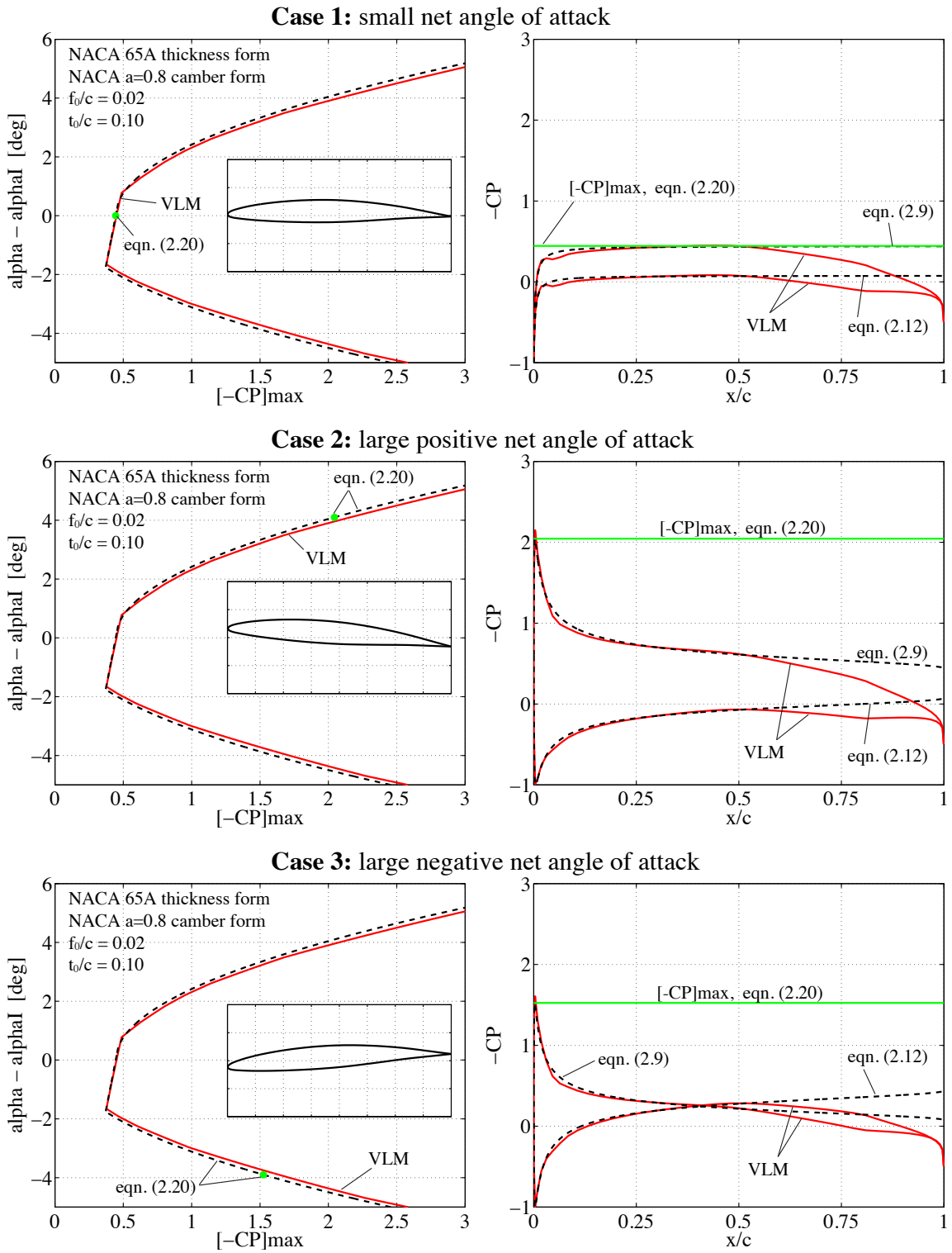

Figure 2: Brockett diagram and pressure distributions, comparing `VLM` code versus analytic $C_p(x/c)$ equations (2.9) and (2.12), and $[-C_p]_{\max}$ equation (2.20).

Case 3: large negative net angle of attack (non-linear region). Here, $[-C_p]_{\max}$ is located on the lower surface at

$$x/c = \frac{A_3^2}{A_3^2 + A_4^2(1+2c/r_\ell)^2} \tag{2.18}$$

(A_3 and A_4 are both positive) and similar to case 2,

$$[-C_p]_{\max} \approx A_3^2 + A_4^2(2c/r_\ell) - 1 \tag{2.19}$$

This is the case when, by quadratic formula,

$$A_4 > \frac{-2A_1 + \sqrt{(2A_1)^2 - 4(2c/r_\ell)(A_3^2 - A_1^2)}}{2\cdot(2c/r_\ell)}$$

Thus, the bucket diagram can be formed as follows

$$[-C_p]_{\max} \approx \begin{cases} A_1^2 + 2A_1A_2 - 1 & \text{(case 1)} \\ A_1^2 + A_2^2(2c/r_\ell) - 1 & \text{(case 2)} \\ A_3^2 + A_4^2(2c/r_\ell) - 1 & \text{(case 3)} \end{cases} \tag{2.20}$$

The bucket diagram can also be computed numerically, given the 2D geometry. The VLM code employed herein (Kerwin, 2007), represents the blade using point sources and vortices distributed along the chord line, and the Lighthill leading edge correction is employed as well (Lighthill, 1951). Figure 3 shows good agreement between $[-C_p]_{\max}$ computed by VLM and by (2.20) for a wide range of thickness ratios.

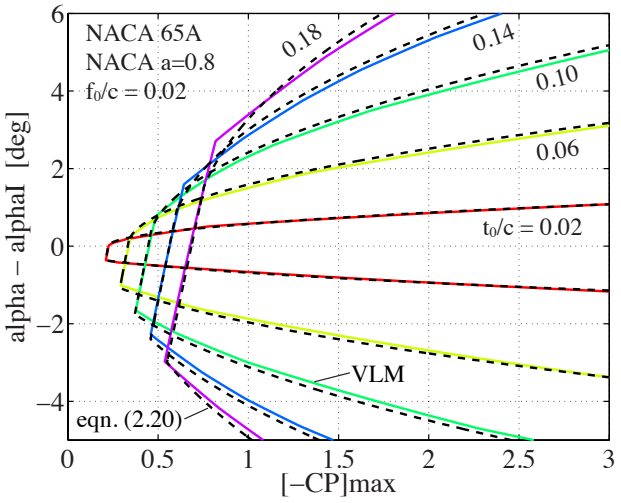

Figure 3: Brockett diagram: VLM '–'; equation (2.20) '- -'. Colors distinguish thickness to chord ratios $t_0/c \in [0.02, 0.18]$ as shown.

Equation (2.20) can be rearranged in terms of the blade loading (Γ, V^*) and the geometry (c,τ) as follows. Since camber is fixed at the (endurance speed) design point, $C_{L_I} = C_{L_e} = \dfrac{2\Gamma_e}{V_e^* c}$. Also, one can approximate the lift coefficient at an off-design point by $C_L \approx C_{L_I} + 2\pi(\alpha - \alpha_I)$. Thus, define

$$a_1 \equiv 1.20 \text{ for 'NACA 65A'} \tag{2.21}$$

$$a_2 \equiv \frac{\Gamma_e}{V_e^*(1+a)} \tag{2.22}$$

$$a_3 \equiv \frac{1}{2\pi}\left(\frac{2\Gamma_m}{V_m^*} - \frac{2\Gamma_e}{V_e^*}\right) \tag{2.23}$$

such that

$$[-C_p]_{\max} \approx \begin{cases} \left(1 + a_1\tau + \dfrac{a_2}{c}\right)^2 + 2\left(1 + a_1\tau + \dfrac{a_2}{c}\right)\dfrac{a_3}{c} - 1 \\ \left(1 + a_1\tau + \dfrac{a_2}{c}\right)^2 + \dfrac{a_3^2}{c^2\tau^2}\dfrac{2}{\rho_\ell} - 1 \\ \left(1 + a_1\tau - \dfrac{a_2}{c}\right)^2 + \dfrac{a_3^2}{c^2\tau^2}\dfrac{2}{\rho_\ell} - 1 \end{cases} \tag{2.24}$$

A design procedure that employs (2.24) can now be summarized. For given loading, constants $\{a_1, a_2, a_3\}$ can be computed. Then contours of $[-C_p]_{\max}$ can be found for several $\{c,\tau\}$. The optimum design minimizes c while $[-C_p]_{\max} = \sigma$. This method is discussed in detail in §3.3.3.

3.0 DESIGN OPTIMIZATION METHODS

Herein, we consider the optimization of circulation, camber, and thickness for given propeller design parameters. In the standard approach (Figure 4a), only the *endurance speed* is considered. The circulation and chord optimization procedures are performed sequentially, iterating until circulation converges (which, practically-speaking, implies that chord has converged as well). In this procedure, the chord lengths can be set to prevent cavitation at the endurance speed, but this does not ensure that cavitation is prevented at the ship's *maximum speed*. Also, this method does not typically involve blade thickness optimization.

In the present design method (Figure 4b), both the *endurance speed* and *maximum speed* are considered automatically. An inner loop runs to optimize the circulation distribution at the *endurance speed*, and an outer loop runs to optimize the chord and thickness to prevent cavitation at the *maximum speed*. When both the circulation and chord have converged, the blade design is complete, and no further modifications are necessary. This design optimization procedure is an automated, deterministic design approach, which enables parametric studies comparing various design inputs, such as propeller diameter, *endurance speed* rotation rate, and number of blades.

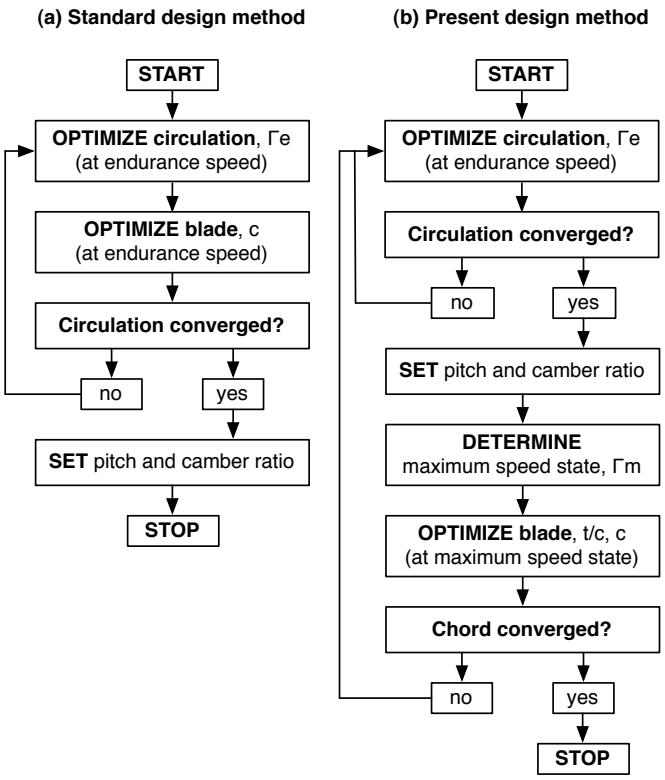

Figure 4: Propeller design optimization methods.

3.1 Circulation optimization

Circulation optimization is performed following the procedure of Kerwin, Coney, and Hsin (1986), which is to find the set of M vortex panel circulations that produce the least torque for a specified (endurance speed) thrust, $T = T_e$. They form an auxiliary function, $H = Q + \lambda_1(T - T_e)$, where λ_1 is a Lagrange multiplier and Q is the torque, and they find the optimum Γ by setting the partial derivatives of H to zero

$$\frac{\partial H}{\partial \Gamma_{(i)}} = 0, \quad \frac{\partial H}{\partial \lambda_1} = 0 \tag{3.1}$$

which is a system of $M+1$ equations for as many unknowns $\{\Gamma_{(i=1\ldots M)}, \lambda_1\}$. For a given chord distribution, $c(r)$, this nonlinear system of equations can be solved iteratively.

3.2 Off-design analysis

In the procedure outlined in Figure 4b, we are given a *maximum ship speed*, V_m, and required thrust, T_m, and we now need to determine the required rotation speed, ω_m so we can use the procedure in §2.1 to determine the max-speed loading $\{\Gamma_m, V_m^*, \text{etc.}\}$, which is required for blade shape optimization. From the given information, we can formulate the required thrust coefficient (C_{T_m} or K_{T_m})

$$C_{T_m} = \frac{T_m}{\frac{1}{2}\rho V_m^2 \pi R^2} = \frac{8}{\pi}\frac{K_{T_m}}{J_m^2} \tag{3.2}$$

We now present a fast algorithm to determine the required advance coefficient $J_m = \dfrac{\pi V_m}{\omega_m R}$, such that $C_T(J_m) = C_{T_m}$.

First note that for most propellers, the $K_T(J)$ curve is nearly linear.

$$K_{T_m} \equiv K_T(J_m) \approx K_T(J) + K_T'(J)\cdot(J_m - J) \tag{3.3}$$

where $K_T' \equiv \frac{dK_T}{dJ}$ can be estimated using finite differences between two prior $K_T(J)$ values. Thus,

$$C_{T_m} \approx \frac{8}{\pi}\frac{K_T(J) + K_T'(J)\cdot(J_m - J)}{J_m^2} \tag{3.4}$$

Given current J, $K_T(J)$, and $K_T'(J)$ values, the next guess for J_m is then

$$J_m \approx \frac{K_T' + \sqrt{(K_T')^2 - 4(\frac{\pi}{8}C_{T_m})(K_T'\cdot J - K_T)}}{2(\frac{\pi}{8}C_{T_m})} \tag{3.5}$$

This typically only takes a few iterations to converge on the J_m needed such that $C_T(J_m) = C_{T_m}$.

3.3 Chord length optimization

Three chord length optimization methods are now presented. Methods 1 and 2 must be used with procedure (Figure 4a), while method 3 is used with (Figure 4b). A cavitation margin, μ, can be implemented in methods 2 and 3 by replacing σ with $\mu\sigma$ in the following equations.

3.3.1 Method 1: maximum lift coefficient

Since lift coefficient is related to the pressure difference across the blade section, it is a proxy measure of cavitation performance. Typically, to mitigate cavitation inception (particularly at the root and tip) section lift coefficients are limited to a maximum allowable distribution:

$$C_{L_{\max}}(r) = 0.5 + (0.2 - 0.5)\frac{r - R_{\text{hub}}}{R_{\text{tip}} - R_{\text{hub}}} \tag{3.6}$$

which yields 0.5 at the hub and 0.2 at the tip. Thus, the optimum chord length is

$$c = \frac{2\,\Gamma_e}{V_e^* C_{L_{\max}}} \tag{3.7}$$

While this simple method ensures adequate loading at the (endurance speed) design point, it does not necessarily prevent cavitation, nor does it prescribe the optimum thickness distribution.

3.3.2 Method 2: Brockett diagram map

Coney (1989) sets the chord distribution based on the following equation:

$$\sigma(r) = 26.67\frac{f_0^2}{c^2} + 8.09\frac{f_0}{c} + 10.0\frac{f_0}{c}\frac{t_0}{c} + 3.033\frac{t_0}{c} \tag{3.8}$$

which approximately sets $[-C_p]_{\max} = \sigma$ at the transition between case 1 and case 2 of the Brockett bucket diagram; thus, it provides the optimum angle of attack envelope for the given thickness, camber (2.1), and cavitation number (2.4).

This method can only be used to optimize the chord

distribution at the *endurance speed*, as equation (2.1) sets the blade camber for the required loading at this design point, and equation (3.8) implicitly assumes that the angle of attack of the blade section is the ideal angle of attack, to center the blade section in its Brockett bucket curve. This method also requires $t_0(r)$ to be specified.

3.3.3 Method 3: linear foil theory C_p

Using equation (2.24) to estimate $[-C_p]_{\max}$, we are now equipped to optimize both c and τ to prevent cavitation at the *maximum speed*, for which we have computed Γ_m, V_m^*.

Generally for *displacement-hull vessels*, $C_{T_m} > C_{T_e}$ (which requires $J_m < J_e$); thus, $\alpha - \alpha_I > 0$, and either case 1 or case 2 will apply. Contours of $[-C_p]_{\max}$ for case 1 and case 2 are shown in Figure 5, with $[-C_p]_{\max} = \sigma$ highlighted in red.

For case 2, equations (2.6) and (2.24) yield

$$\left(1 + a_1\tau + \frac{a_2}{c}\right)^2 + \frac{a_3^2}{c^2\tau^2}\frac{2}{\rho_\ell} - 1 = \sigma \tag{3.9}$$

which is plotted in red in Figure 5. It is clear from Figure 5 that there is an optimum τ that minimizes c. Thus, a second constraint equation is that $\dfrac{dc}{d\tau} = 0$ while traversing the contour defined by (3.9):

$$2a_1\left(1 + a_1\tau + \frac{a_2}{c}\right) - 2\frac{a_3^2}{c^2\tau^3}\frac{2}{\rho_\ell} = 0 \tag{3.10}$$

Equations (3.9) and (3.10) form a deterministic set of equations that prescribe (c, τ) given $(\Gamma_e, V_e^*, \Gamma_m, V_m^*,$ and $\sigma)$. The intersection of (3.9) and (3.10) yields the optimum c and τ, which is plotted as a '•' in Figure 5.

For case 1, equations (2.6) and (2.24) yield

$$\left(1 + a_1\tau + \frac{a_2}{c}\right)^2 + 2\left(1 + a_1\tau + \frac{a_2}{c}\right)\frac{a_3}{c} - 1 = \sigma \tag{3.11}$$

As shown in Figure 5, setting $\tau = 0$ minimizes the chord length, but this is not possible due to strength considerations. If the τ from case 2 is selected, then (3.11) yields the optimum chord. The larger of the chord lengths required by case 1 and case 2 is then selected.

Case 1: small net angle of attack.

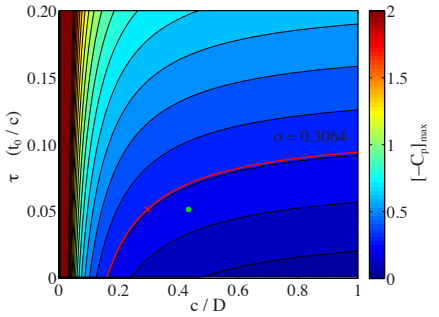

Case 2: large positive net angle of attack.

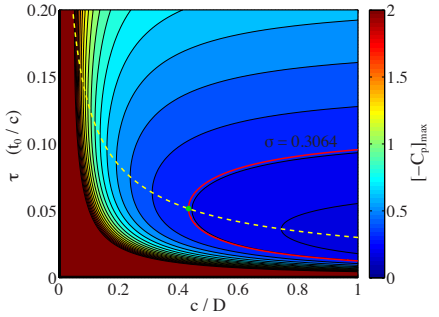

Figure 5: Contours of $[-C_p]_{\max}$ (2.24), with $[-C_p]_{\max} = \sigma$ (3.9) marked in red, constraint equation (3.10) '--', and optimum (c, τ) '•'.

Generally for *planing-hull vessels*, $C_{T_m} < C_{T_e}$ (which requires $J_m > J_e$); thus, $\alpha - \alpha_I < 0$, and either case 1 or case 3 will apply. Case 1 has already been discussed. For case 3, equations (2.6) and (2.24) yield

$$\left(1 + a_1\tau - \frac{a_2}{c}\right)^2 + \frac{a_3^2}{c^2\tau^2}\frac{2}{\rho_\ell} - 1 = \sigma \tag{3.12}$$

Qualitatively, contours of $[-C_p]_{\max}$ for case 3 are similar to those for case 2. Likewise, equation (3.12) behaves similarly to (3.9), and the resulting constraint equation ($\frac{dc}{d\tau} = 0$) is

$$2a_1\left(1 + a_1\tau - \frac{a_2}{c}\right) - 2\frac{a_3^2}{c^2\tau^3}\frac{2}{\rho_\ell} = 0 \tag{3.13}$$

Analogous to equations (3.9) and (3.10) for the displacement-hull vessel, the intersection of (3.12) and (3.13) yields the optimum c and τ for the planing-hull vessel.

Surprisingly, this procedure naturally results in $\tau(r)$ that varies nearly linearly along the span of the blade. The required chord length at the root is quite short, and the blade is quite thin at the root, which is not a practical design solution. In particular, the resulting blade does not meet the American Bureau of Shipping (ABS) standards for blade thickness at the root. Thus, an additional modification to the blade shape is required.

3.3.4 ABS thickness requirement

The American Bureau of Shipping standard requires minimum blade thickness to meet strength requirements (ABS, 2007). Herein, we consider the ABS requirement for fixed-pitch propellers (ABS, 2007, part 4-3-3, subsection 5.1, p.241). The formula is quite complex but can be simplified as follows:

$$\frac{t_{0_{25}}}{D}\sqrt{\frac{c_{25}}{D}} \approx T_1 \tag{3.14}$$

where

$$T_1 \equiv \frac{T_0}{10^6}\sqrt{\frac{1+6/\bar{p}_{70}+4.3\bar{p}_{25}}{1+1.5\bar{p}_{25}}\frac{\mathcal{P}_r}{fN_rD^3\mathcal{Z}}}$$

and $T_0 \equiv 1.025\cdot 337/\sqrt{0.1}$ in SI units; c is the section chord length [m]; t_0 is the maximum section thickness [m]; $\bar{p}$ is the pitch to diameter ratio; D is the diameter [m]; $f \equiv 2.62$ for nickel-aluminum bronze; N_r is the rotation rate [RPM] at *engine rated speed*; $\mathcal{P}_r$ is the power [W] at *engine rated speed*; $\mathcal{Z}$ is the number of blades; and the subscripts 25 and 70 indicate $r/R = 0.25$ and 0.70, respectively. Herein, we take the *engine rated speed* condition to be the the *ship maximum speed* condition: $\mathcal{P}_r \equiv \mathcal{P}_m = 0.5\rho V_m^3 \pi R^2 C_{\mathcal{P}_m}$ and $N_r \equiv N_m = 60V_m/(J_m D)$.

For a given thickness ratio distribution (namely, t_0/c at $r = 0.25R$), equation (3.14) can be used to find the required thickness at the 0.25 radius:

$$\frac{t_{0_{25}}}{D} \approx \left(T_1\sqrt{(t_0/c)_{25}}\right)^{2/3} \tag{3.15}$$

To meet this requirement, the thickness distribution is modified as shown in Figure 6. The new thickness distribution is linear from $r/R = 0.25$ to the point where it intersects the old thickness distribution tangentially and then follows the old thickness distribution out to the tip. While holding t_0/c constant, chord is increased to meet this new thickness distribution.

$$\left(\frac{c}{D}\right)_{\text{new}} = \frac{(t_0/D)_{\text{ABS}}}{(t_0/c)_{\text{old}}} \tag{3.16}$$

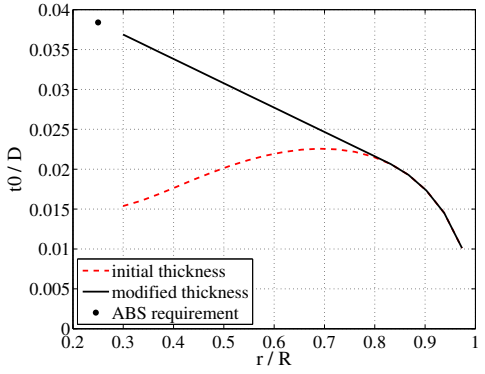

Figure 6: Thickness modification to satisfy (3.15).

4.0 ILLUSTRATIVE EXAMPLE

An illustrative example is presented that combines the performance specifications for the DDG51 destroyer-class vessel (Tsai et al, 1994) with those of David Taylor Model Basin propeller 5168 (Chesnakas and Jessup, 1998). DTMB 5168 is a representative modern surface ship propeller, suitable for the DDG 51 vessel. Although DTMB 5168 is a controllable-pitch propeller, the example herein considers designing a fixed-pitch propeller (as the present design method is restricted to fixed-pitch propellers). The design specifications for propeller 5168 are a representative set of specifications for this example displacement-hull vessel. The primary design parameters are listed in Table 2. Where possible, the design parameters follow those of propeller 5168, namely $\mathcal{Z}$, D, and D_{hub}/D. The thrust requirements at the $V_e = 20$ knot *endurance speed* and $V_m = 30$ knot *maximum speed* were formed by multiplying the values in (Tsai et al, 1994) by 1.09, in order to match the K_T requirement at the endurance speed with that of propeller 5168. The rotation rate at endurance speed was then chosen to match the advance ratio of propeller 5168.

The inflow velocity profile was assumed uniform ($V_a/V_s = 1$ and $V_t/V_s = 0$ for all blade sections). Although propeller 5168 employs rake and skew, these were set to zero for this study. The section drag coefficient was assumed to be $C_D = 0.008$ for all blade sections. Blade sections were formed using the 'NACA a=0.8' meanline and 'NACA 65A' thickness forms.

Four propellers were designed in this study, as summarized in Table 3. The 'Epps w/ ABS' propeller employs the present design methods detailed in Figure 4b, §3.3.3, and §3.3.4. To highlight the effect of the ABS requirement, the 'Epps w/o ABS' propeller was designed using only Figure 4b and §3.3.3. The standard design method (Figure 4a) yields the 'CLmax' propeller (§3.3.1) or the 'Coney' propeller (§3.3.2). The 'CLmax' and 'Coney' propellers used the thickness distribution (t_0/D) from the 'Epps w/ ABS' design.

Table 2: Propeller design input parameters.

Parameter	Description
$\mathcal{Z} = 5$	number of blades
$D = 5.18$ m	diameter (17 ft)
$D_{\text{hub}} = 1.46$ m	hub diameter ($0.2819D$)
$N_e = 93.8$ RPM	rotation rate at V_e
$V_e = 10.29$ m/s	endurance speed (20 kts)
$T_e = 4.159$e5 N	thrust at V_e
$V_m = 15.43$ m/s	max speed (30 kts)
$T_m = 1.38$e6 N	thrust at V_m
$\rho = 1025$ kg/m^3	sea-water density
$H = 6.31$ m	shaft depth (20.7 ft, at draft)
$M = 20$	number of vortex panels
$J_e = 1.2701$	advance coefficient at V_e
$C_{T_e} = 0.3637$	thrust coefficient at V_e
$C_{T_m} = 0.5364$	thrust coefficient at V_m

Table 3: Summary of design methods.

Name	Design methods
'Epps w/ ABS'	Figure 4b, §3.3.3, §3.3.4
'Epps w/o ABS'	Figure 4b, §3.3.3
'CLmax'	Figure 4a, §3.3.1
'Coney'	Figure 4a, §3.3.2

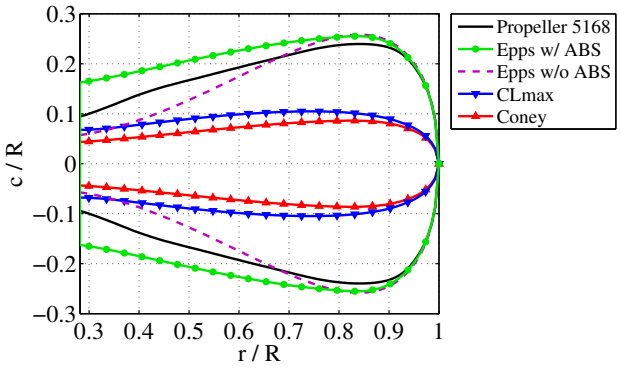

Figure 7: Chord distribution.

The blade outline for the four propellers and propeller 5168 are shown in Figure 7. The 'Epps w/ ABS' design well replicates Navy propeller 5168, which validates that the procedures in §3.3.3 and §3.3.4 yield a realistic blade outline. The 'Epps w/o ABS' propeller has a similar tip but much shorter chord lengths (and thicknesses, as shown in Figure 8d) near the root. This illustrates how the ABS thickness requirement augments the required blade shape. Both the 'CLmax' and 'Coney' propellers have much shorter chord lengths, as these are only designed to mitigate cavitation at the endurance speed.

Figure 8 shows additional comparisons between these four propeller designs. Figure 8a shows that the endurance speed circulation loading is nearly identical for the four designs; this is because viscous parasitic drag forces are small ($F_v = \frac{1}{2}\rho(V^*)^2 C_D c$, with $C_D = 0.008$), so nearly the same circulation loading is required regardless of the chord lengths. Figure 8b shows lift coefficient. Interestingly, the 'Epps w/ ABS' procedure results in a nearly linear C_L distribution over the span of the blade. In this case, these lift coefficients are about half of those that we arbitrarily chose for the 'CLmax' propeller. This shows that while the 'CLmax' procedure (§3.3.1) is sound, it doesn't necessarily mitigate cavitation. Figs. 8c and 8d show the thickness ratio and thickness, respectively. Note that the 'Epps w/ ABS' propeller has nearly the same thickness distribution as P5168, providing another validation for this method. The 'Epps w/o ABS' has a slightly different t_0/c as the 'Epps w/ ABS'; although t_0/c is fixed in the ABS procedure (§3.3.4) during each optimizer iteration, the optimizer converged on slightly different results after multiple iterations. Since the 'CLmax' and 'Coney' propellers used the t_0/D from the 'Epps w/ ABS' design but have smaller chord lengths, the t_0/c distributions are much larger and are in fact impractical. This emphasizes the advantage o the present procedure, which optimizes both thickness and chord with no *a priori* assumptions.

Figure 9 compares the suction-side cavitation performance of the 'Epps w/ ABS' propeller to the 'CLmax' propeller. The pressure distributions were computed here using the 2D `VLM` solver applied to each blade section. The top panel shows that both are cavitation free at the endurance speed. The lower panel shows that while the 'Epps w/ ABS' propeller is still cavitation free at the maximum speed – as expected – the 'CLmax' propeller shows significant suction-side cavitation.

Finally, Figure 10 compares the 3D geometry of P5168 to the 'Epps w/ ABS' propeller. For comparison, the rake and skew distribution of P5168 were used for both figures. These figures show that the 'Epps w/ ABS' procedure (Figure 4b, §3.3.3, and §3.3.4) clearly yields a realistic and representative propeller blade design.

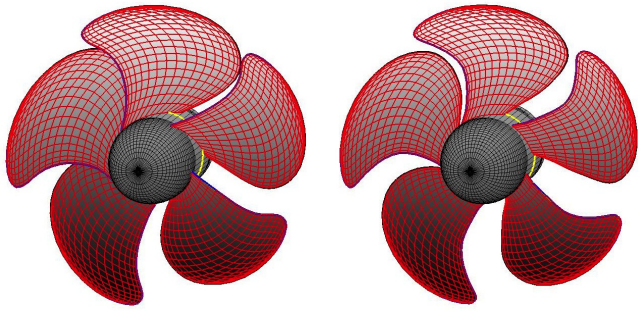

(a) (b)

Figure 10: Propeller geometry: (a) 'Epps w/ ABS' design using propeller 5168 skew; (b) actual DTMB propeller 5168.

The outputs of the method in this paper are the propeller chord and thickness distributions (in addition to the circulation, pitch, and camber distributions derived from the standard lifting line design method); rake and skew could then be applied to the propeller, as illustrated here. The known limitation of the lifting line method is that the predicted pitch and camber distributions will not actually yield the desired circulation distribution; advance design techniques, incorporating the use of lifting surface or panel methods could be used to modify the pitch and camber distributions of the 'Epps w/ ABS' blade geometry to achieve the desired 'Epps w/ ABS' circulation distribution (Greeley and Kerwin, 1982).

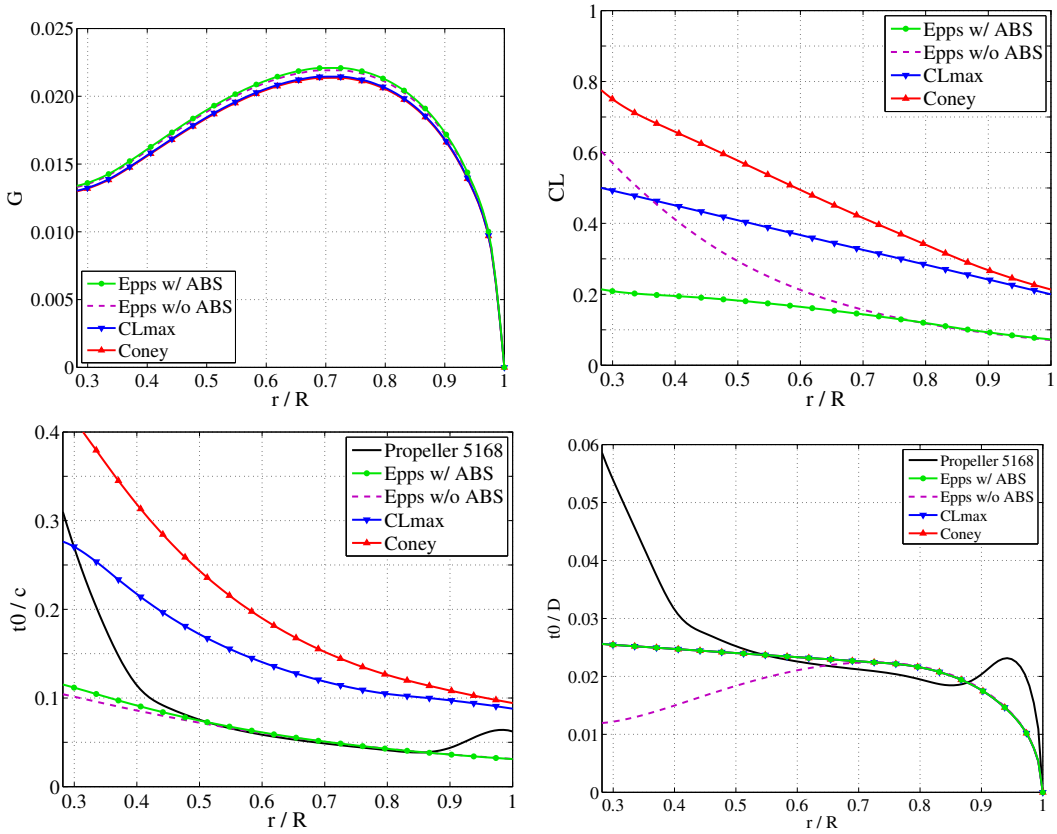

Figure 8: Performance of the four propeller designs, where $G = \dfrac{\Gamma_e}{2\pi R V_e}$ and $C_L = \dfrac{2\Gamma_e}{(V_e^*)c}$.

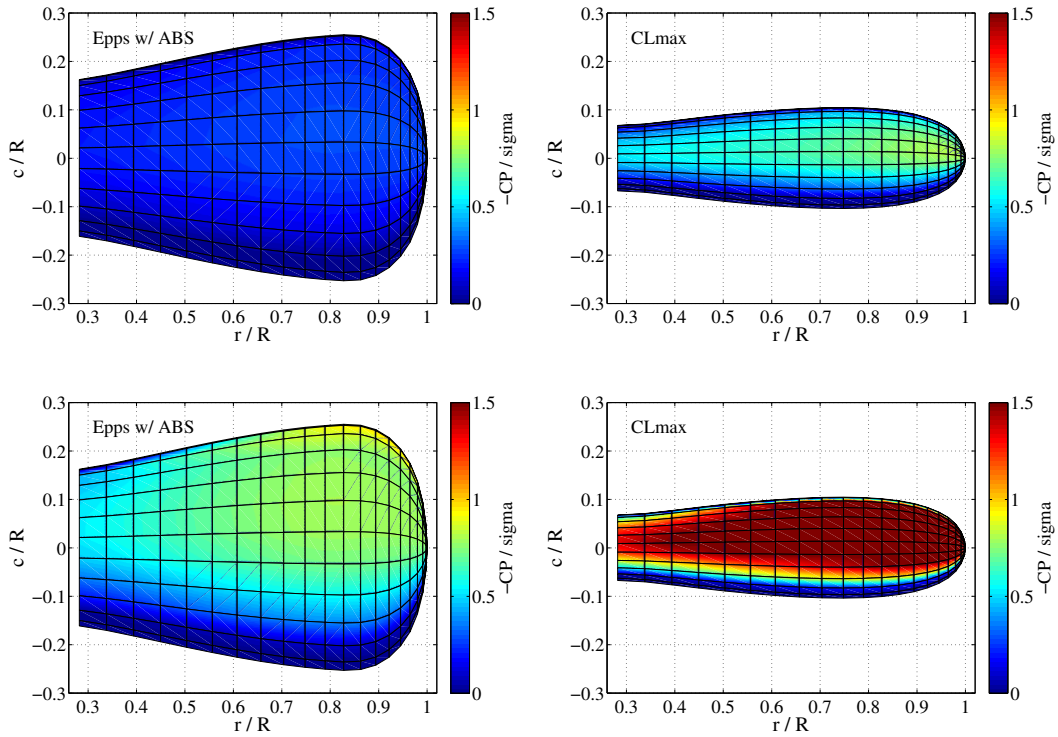

Figure 9: Suction-side pressure distribution shows cavitation performance: (top) endurance speed, (bottom) maximum speed; (left) 'Epps w/ ABS' design, (right) 'CLmax' design.

4.1 Parametric design study

We now investigate the effect of varying certain parameters in our design exercise. In particular, we consider the effects of maximum speed V_m, required thrust coefficient at maximum speed C_{T_m}, and shaft submergence depth. In this study, the 'Epps w/ ABS' procedure (Figure 4b, §3.3.3, and §3.3.4) is used to design several additional propellers.

Figure 11a shows the effect of varying the maximum speed V_m while holding the maximum thrust coefficient C_{T_m} constant. Not surprisingly, increasing V_m increases both the required chord length and thickness distributions, with the largest c/R and t_0/c distributions shown in Figure 11a corresponding to the largest V_m considered. The nominal design (Figs. 7 and 8) is shown for reference. Interestingly, as V_m is reduced to V_e, the 'Epps w/ ABS' procedure results in nearly the same chord distribution as the Coney (1989) procedure, for radii near the tip ($r/R > 0.8$).

Figure 11b shows the effect of varying the required maximum thrust coefficient C_{T_m}, while holding V_m fixed. Again the results are not surprising; increasing C_{T_m} increases the required chord and thickness.

Finally, Figure 11c shows the effect of varying the shaft submergence depth H. This parameter only affects the cavitation number, via (2.4). Decreasing the shaft submergence depth also increases the required chord and thickness. However, the effect of H is less pronounced than that of C_{T_m} or V_m.

5.0 CONCLUSION

This paper presents an analytic estimate of the minimum pressure coefficient on a 2D non-cavitating hydrofoil (2.20). This estimate was used to develop an analytic approximation to the cavitation bucket diagrams typically used in marine propeller design. Further, a novel design procedure was developed to optimize blade loading for maximum efficiency at an endurance speed while mitigating cavitation at a maximum speed (Figure 4b). To enable this procedure, a method was developed to efficiently find the advance coefficient needed to produce a required thrust coefficient (§3.2). Using the analytic estimate of the minimum pressure coefficient, it was found that an optimum chord length and thickness ratio exist, such that chord is minimized while the negative pressure coefficient does not exceed the cavitation number (§3.3.3). Finally, we illustrated this novel optimization procedure in application the DDG51 destroyer-class vessel (§4.0).

The present methods are coded in the OPENPROP suite (Epps and Kimball, 2013a) and are readily-available for academic and industrial use. This work extends the capabilities of OPENPROP to high-speed ship propulsion applications.

The design optimization procedure developed herein is an automated, deterministic design approach, which enables parametric studies comparing various design inputs, such as propeller diameter, endurance speed rotation rate, and number of blades.

This article did not consider the case of a propeller operating in spatially-varying axial inflow. This case actually is quite important, as a ship wake typically produces an axial velocity defect in the "10 o'clock – 2 o'clock region" of the propeller inflow. This axial velocity defect results in local angle of attack changes at each blade section, which ultimately may lead to cavitation. The methods presented in this work can, in principle, be extended to include rough estimates of cavitation for propellers operating in this non-uniform inflow as it rotates through the ship wake field. Cavitation estimates could be computed at several blade positions using the 'analytical Brockett diagram' method presented in §2.3. However, since the methods presented herein assume a fully-wetted blade, estimates of cavitation area on a partially-cavitating blade would be very rough. The extension of the present methods to non-uniform inflow is the subject of ongoing work.

The present method is intended for preliminary design work at the lifting line model stage. Thus, the output blade geometry (camber and pitch) suffers the known limitations of lifting line model. A more complete numerical method would couple the present lifting line model with a lifting surface blade design model, such that a more accurate blade geometry and pressure distribution can be computed for each candidate propeller design. Combining lifting line, lifting surface, and the optimization methods presented herein would provide an automated design procedure to determine an optimum propeller geometry including number of blades and diameter, as well as the chord, pitch, camber, and thickness distributions.

ACKNOWLEDGEMENTS

This work was supported by the Office of Naval Research (N00014-11-1-0598), the MIT Sea Grant College Program (NA060AR4170019 and NA10OAR4170086), and Mr. Robert Damus of Project Ocean. We also wish to thank the Thayer School of Engineering at Dartmouth College for providing additional support.

The authors would like to thank the anonymous peer reviewers for their insightful comments, which has improved the quality of this manuscript.

REFERENCES

Abbott, I.H. and von Doenhoff, A.E. (1959) Theory of Wing Sections. Dover.

ABS (2007) Rules for Building and Classing Steel Vessels. American Bureau of Shipping.

Brizzolara S, Villa D, Gaggero S (2010) A systematic comparison between rans and panel methods for propeller analysis. In: 9th International Conference on Hydrodynamics (ICHD2010)

Brockett, T.E. (1966) "Minimum Pressure Envelopes for Modified NACA-66 Sections with NACA a=0.8 Camber

(a) Study 1: maximum speed V_m

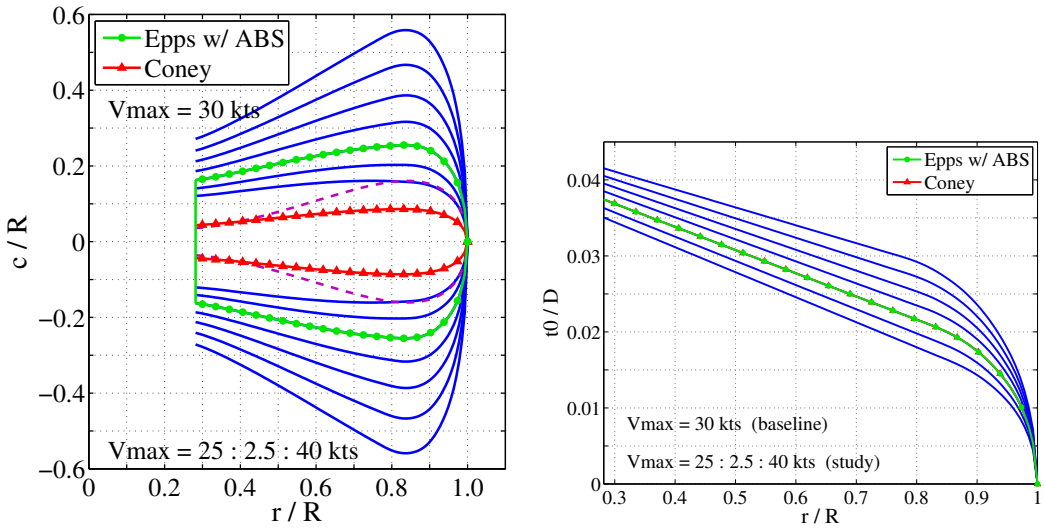

(b) Study 2: maximum thrust coefficient C_{T_m}

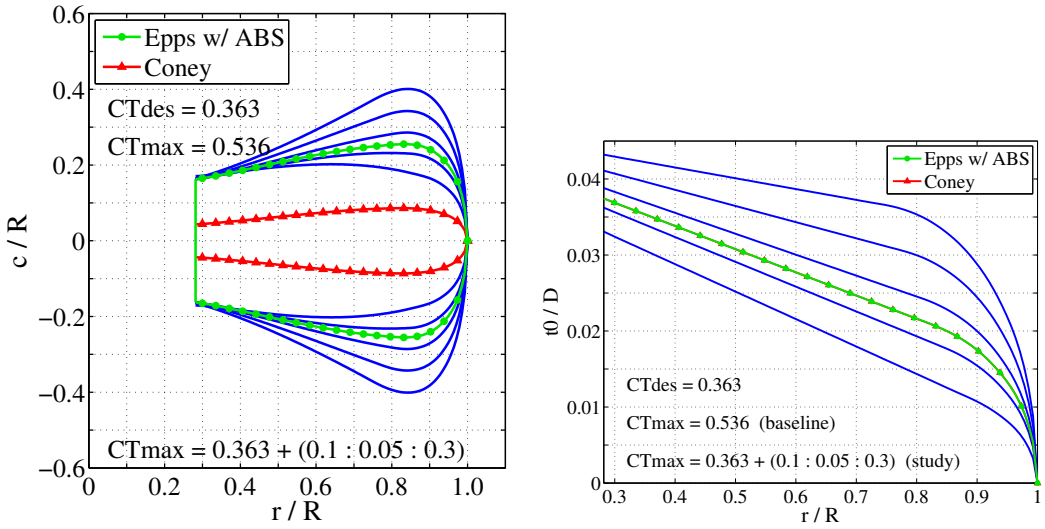

(c) Study 3: shaft submergence depth H

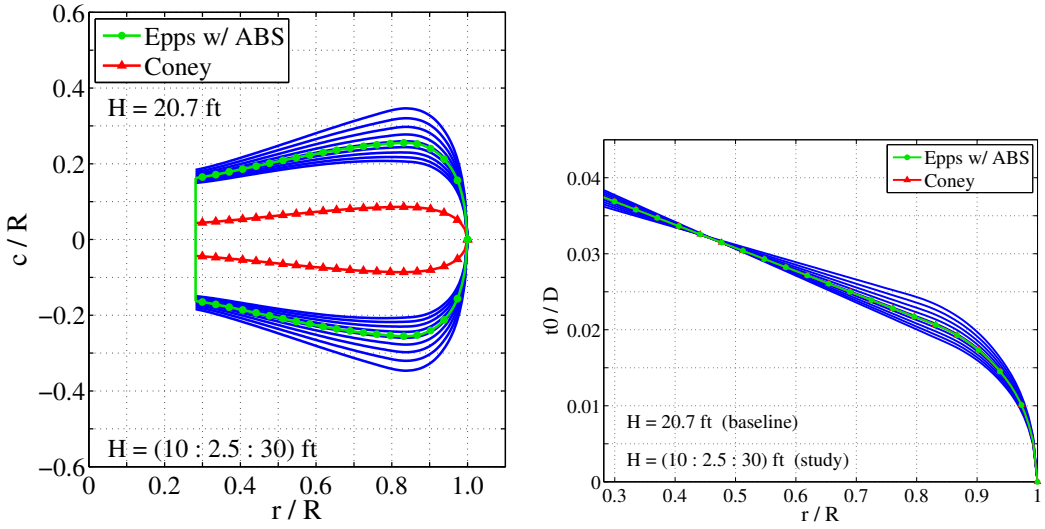

Figure 11: Parametric design study showing required blade outline (c/R and t_0/D) versus (a) maximum speed V_m, (b) required thrust at the maximum speed C_{T_m}, and (c) shaft submergence depth H.

and Buships Type I and Type II Sections". DTMB Report 1780, Carderock, MD.

Chesnakas, C. and Jessup, S. (1998) “Cavitation and 3-D LDV Tip-Flowfield Measurements of Propeller 5168". Tech. rep., Naval Surface Warfare Center, Carderock, MD.

Coney, W.B. (1989) A Method for the Design of a Class of Optimum Marine Propulsors. PhD thesis, MIT, Cambridge, MA.

Epps, B.P. (2010a) An Impulse Framework for Hydrodynamic Force Analysis: Fish Propulsion, Water Entry of Spheres, and Marine Propellers. PhD thesis, MIT, Cambridge, MA.

Epps B, Kimball R (2013a) OPENPROP V3: Open-source software for the design and analysis of marine propellers and horizontal-axis turbines. URL http://engineering.dartmouth.edu/epps/openprop

Epps B, Kimball R (2013b) Unified rotor lifting line theory. Journal of Ship Research 57(4):1–21

Greeley DS, Kerwin JE (1982) Numerical methods for propeller design and analysis in steady flow. SNAME Transactions 90

Kerwin J (2007) Hydrofoils and propellers. MIT course 2.23 notes

Kerwin, J.E. and Hadler, J.B. (2010) Principles of Naval Architecture: Propulsion. SNAME.

Kerwin, J.E.; Coney, W.B.; Hsin, C.Y. (1986) “Optimum Circulation Distributions for Single and Multi-Component Propulsors." Twenty-First American Towing Tank Conference, p. 53 – 62.

Kinnas S, Choi JK, Lee H, Young Y, Gu H, Kakar K, Natarajan S (2002) Prediction of cavitation performance of single or multi-component propulsors and their interaction with the hull. SNAME Transactions 110:215–244

Lerbs, H.W. (1952) “Moderately Loaded Propellers with a Finite Number of Blades and an Arbitrary Distribution of Circulation". SNAME Transactions. vol. 60.

Lighthill, M.J. (1951) “A New Approach to Thin Aerofoil Theory”. The Aeronautical Quarterly **3**(2):193–210.

Tsai, S.J.; Hopkins, B.; Stenson, R. (1994) “Comparison of Powering Performance Between DDG-51 and Conventional Combatant Hull Forms". Naval Engineers Journal **106**(5):88–99.